CLIFF EROSION AND BOTTOM MORPHODYNAMICS IN A WAVE FLUME

Bastien Caplain[1], Vincent Regard[2] and Dominique Astruc[3]

Abstract

Laboratory experiments were carried out in a monochromatic wave flume. Natural coarse sands are used to represent cliff erosion and bottom morphodynamics with a reasonable time scale. A bottom typology is established as a function of wave forcing, through the wave energy flux F and the surf similarity parameter ξ. The bottom types strongly depend on the surf similarity parameter at the breaker point ξ_b. Steep terraces ($\xi_b > 0.48$), one-bar profiles ($0.42 < \xi_b < 0.48$), gentle terraces ($0.38 < \xi_b < 0.43$) and double-bars profiles ($\xi_b < 0.38$) were observed. Sediment grain diameter change has no noticeable influence on bottom typology. The bottom types depend more on the Dean parameter Ω than on the Shields number at the breaker point Θ_b. Finally, the cliff recession rate linearly increases with F, is not monotonic with ξ and decreases with the grain median diameter of sediment D_{50}.

Key words: morphodynamics, sandy cliff, monochromatic wave flume, recession rate, hydrodynamics, cohesion, granulometry

1. Introduction

Rocky shores occupy about 80% of the coastline of the Earth (Emery and Kuhn, 1980). Cliff erosion is mainly controlled by wave impact but depends likewise on numerous factors (Sunamura, 1992), such as weathering during tidal cycles (Kanyaya and Trenhaile, 2005), bioerosion (Andrews and Williams, 2000), material stratification or fractures. We limited our study to the influence of wave forcing on the cliff erosion by undermining. Rocky coast erosion could be divided into cycles, each one corresponding to three successive phases: (i) the notch creation at the cliff toe by mechanical action of waves (Brossard and Duperret, 2004 ; Erikson et al., 2007), (ii) the cliff fracturation leading to a collapse event (Young and Ashford, 2008) and (iii) the fallen cliff debris progressively evacuated along and across the shore by waves and currents modifying the bottom morphology (de Lange and Moon, 2005 ; Pierre, 2006). In turn, waves and currents are transformed by the bottom morphology. When the debris is fully evacuated, the cycle of cliff erosion begins again (Walkden and Dickson, 2008). In order to reproduce cliff collapses and to observe the erosion process with a reasonnable time scale, wetted coarse sand is used to represent the coastline. Damgaard and Dong (2004) estimated the cliff recession rate in function of wave height and period. However, the mechanisms of cliff erosion and bottom morphodynamics were not analysed in detail whereas Caplain et al. (2011) highlight that sandy cliff recession strongly depends on the bottom morphology. The retroaction between wave energy dissipation and morphology leads to an equilibrium; the morphology then can be described by the Dean number Ω:

$$\Omega = \frac{H_b}{Tw_S} \tag{1}$$

with H_b the breaker height, T the wave period and w_S the sediment fall velocity in water. The Dean number is the ratio of a fall time of a particule H_b/w_S and the wave period T. Some types of bottom morphology in field (e.g. Wright and Short, 1984) and laboratory (e.g. Grasso et al., 2009) have been observed and classified as a function of Dean number Ω. This study is devoted to the experimental analysis of the cliff

[1] Université de Toulouse, IMFT, Allée Camille Soula, 31400 Toulouse, France. caplainbastien@gmail.com
[2] Université de Toulouse, GET, 14 avenue Édouard Belin, 31400 Toulouse, France. regard@get.obs-mip.fr
[3] Université de Toulouse, IMFT, Allée Camille Soula, 31400 Toulouse, France. astruc@imft.fr

recession and the bottom morphodynamics (Figure 1), as a function of the wave climate and the grain size of sediment.

2. Experimental model

We performed the experiments in a monochromatic wave flume of about 5 m long, 14 cm wide and 25 cm high (Figure 1). The offshore water depth was 15 cm. A nearshore slope of tan(β) = 10% was used to model the shore where a wetted sandy cliff was built with a height from water free surface of 8 cm. Three types of sand were used (D_{50} = 0.28-0.41-0.48 mm). Incident wave parameters were estimated by capacitive probes located offshore. Then, in order to detect the free surface and the sand surface, we set up two cameras, one on the side of the flume and the other above the flume. The video sampling rate was close to wave frequency, during about 4 hours and then was decreased to 1/10 of wave frequency until the end of the experiment. Video images are processed to extract both sand and water surfaces position (Figure 2). The monochromatic wave climate is characterized by two parameters, the surf similarity parameter ξ and the incident wave energy flux F which are written:

$$\xi = \frac{\tan(\beta)}{\sqrt{H/\lambda}} \tag{2}$$

$$F = \frac{1}{8}\rho g H^2 C_G \tag{3}$$

with λ the wavelength, ρ the water density, g the gravity acceleration and C_G the group velocity. The hydro-sedimentary parameters chosen are the Dean number Ω (Equation 1) and the breaker Shields number Θ_b.

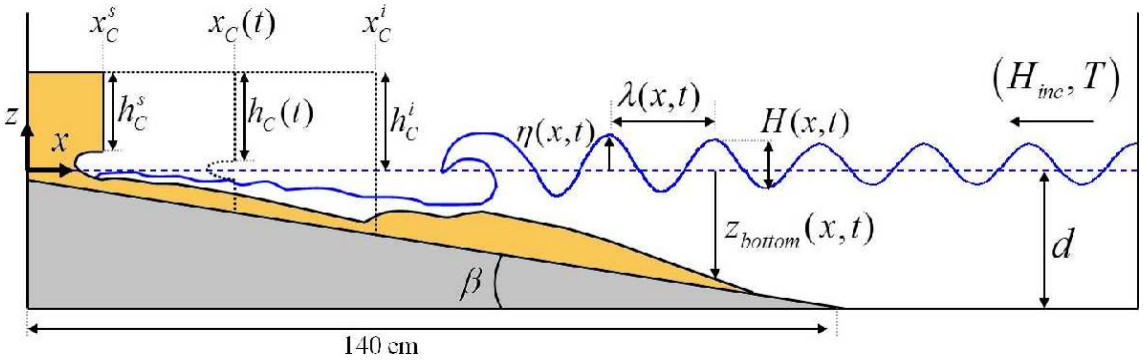

Figure 1. Schematic wave flume. h_C is the cliff height from the water surface at rest, x_C is the initial cliff position, β is the bottom rigid angle and d is the water depth. The (x, z) plan origin is located at the water surface and at the shoreward flume edge.

3. Results

During an experiment, the cliff erosion process occurs on different time scales. At the beginning of the experiments, cliff retreat was very important and collapsed sediment quickly created a sandy platform on the 10% slope (Figure 3: (a) initiation phase), this platform then develops for a few hours and the frequency of cliff collapse decreases (Figure 3: (b) transient phase) until the cliff recession rate tended to 0 and the morphological system tends to stabilize towards a steady state (Figure 3: (c) stabilization phase).

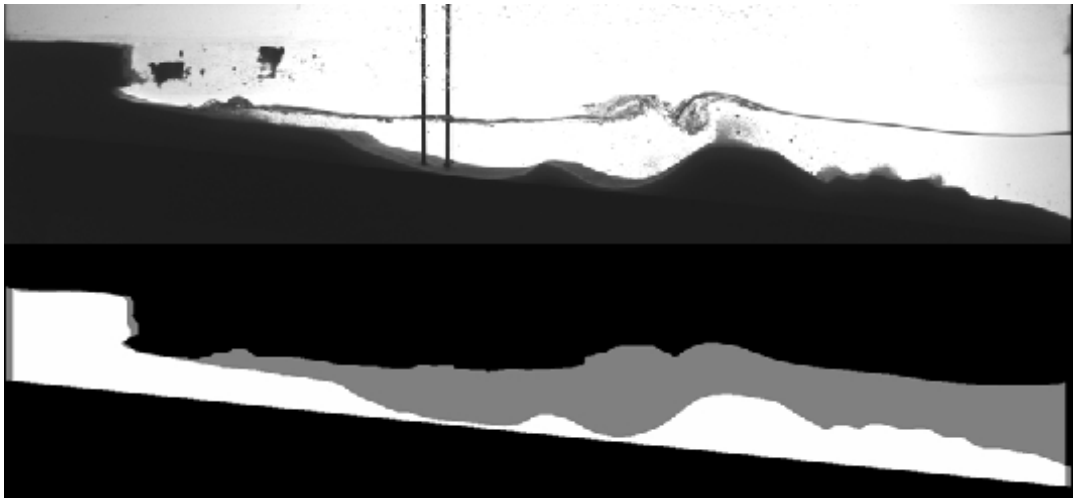

Figure 2. Raw image (up) and corresponding contours of sand surface and water free surface detected (down).

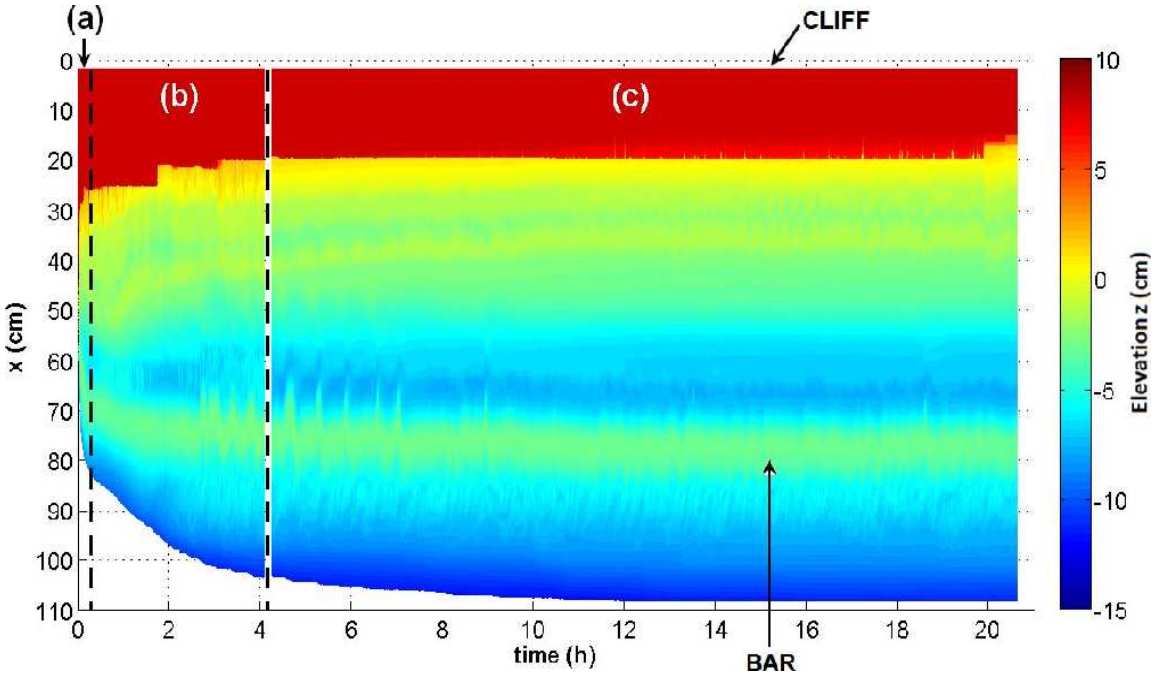

Figure 3. Spatial (x) and temporal (t) evolution of cliff and bottom morphology ((F, ξ) = (1.2 W/m; 0.39) case). Color range indicates the sand surface elevation. Dashed lines separate the three phases of the experiment: (a) initiation, (b) transient and (c) stabilization.

3.1. *Bottom morphodynamics*

We analyse the bottom morphology when the stationary state is reached. Some experiments reached an unsteady state characterized by a sandbar oscillation; we analyze the bottom morphology as an average of the bottom morphologies corresponding to the two extrema of the sandbar position.

Experiments have been carried out for the sand type with the D_{50} = 0.41 mm. We identified four main bottom morphologies based on the outer platform and hydrodynamical characteristics. These bottom types were characterized as a function of wave forcing (F, ξ) (Figure 4). We showed that the bottom morphology

mainly depends on ξ. For the D_{50} = 0.41 mm material, we observed surging breakers on a steep terrace (type T1) for ξ > 0.65, collapsing breakers on a bared profile attached to the inner platform (type T2) for 0.55< ξ <0.6, spilling breakers on gentle terrace (type T3) for 0.5< ξ <0.55. The bottom type T4 was observed for ξ <0.5 and presented two sub-systems, an outer system with a double-bar profile (breaker and splash-up bars, shown in Figure 2) where breaking waves were plunging, and an inner system with a T1, T2 or T3 profile. We consequently propose to subdivide the bottom type4 into types 41 (shown in Figure 2), 42 and 43 according to the inner platform morphology. Some of these bottom morphologies were unsteady characterized by a sandbar oscillation. For the bottom type 3, we distinguish two types of inner platform, one with a small gentle terrace for F < 1 W/m and one with a large steep terrace for F > 1 W/m (Figure 4). Thus, we subdivide the bottom type 3 in 3a for the first case and 3b for the second case.

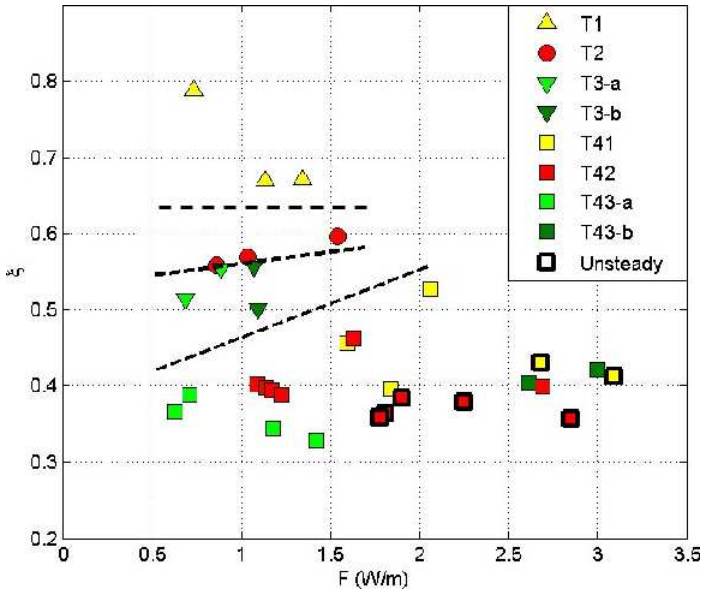

Figure 4. Diagram of bottom typology as a function of wave parameters (F, ξ).

Bottom morphologies are often characterized as a function of wave parameters at the breaker point (e.g. Wright and Short, 1984). We thus establish a classification of bottom morphologies where we replace the incident wave height H by the breaker height H_b. In Figure 5, the bottom typology is represented in the (F_b, ξ_b) diagram with F_b the wave energy flux at the breaker point and ξ_b the surf similarity parameter at the breaker point. We can observe that the bottom type strongly depends on the surf similarity parameter at the breaker point ξ_b. Type 1 profiles are observed for $\xi_b > 0.48$, type 2 profiles for $0.42 < \xi_b < 0.48$, those of type 3 for $0.38 < \xi_b < 0.43$ and those of type 4 for $\xi_b < 0.38$ (cf. Table 1). Profile types 41, 42 and 43 appear to be also dependent on the surf similarity parameter at the breaker point ξ_b. Thus, the profiles 41 are observed for $0.34 < \xi_b < 0.38$, those 42 for $0.3 < \xi_b < 0.34$ and those 43 for $\xi_b < 0.31$ (cf. Table 1). Small symbols shown in Figure 5 correspond to the inner wave parameters at the breaker point of the profile types 41, 42 and 43. We can observe that the types of inner profiles are in line with the characterization made for single system types. This shows that it is possible there are one or no outer system (double-bars and plunging waves), the inner bottom profile only depends on breaking wave forcing.

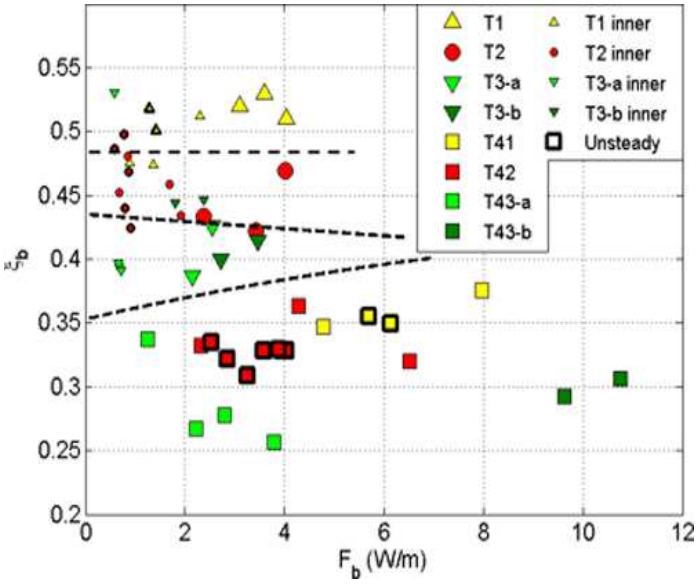

Figure 5. Diagram of bottom typology as a function of wave parameters at the breaker point (F_b, ξ_b).

Table 1. Characteristics of bottom typology.

Bottom Typology	**Outer Platform**	**Inner Platform**	**Breakers types**	**(F_b, ξ_b)**
1	Steep terrace	Steep terrace	Surging	$\xi_b > 0.48$
2	Bared	Steep terrace	Collapsing	$0.42 < \xi_b < 0.48$
3a	Gentle terrace	Gentle terrace	Spilling	$0.38 < \xi_b < 0.43$
3b	Gentle terrace	Steep terrace	Spilling	$0.38 < \xi_b < 0.43$
41	Breaker and	Type 1		$0.34 < \xi_b < 0.38$
42	splash-up	Type 2	Plunging	$0.3 < \xi_b < 0.34$
43	bars	Type 3		$\xi_b < 0.31$

We used two other sands: a finer (D_{50} = 0.28 mm) and a coarser (D_{50} = 0.48 mm). To take into account the grain size change, we characterize the bottom types as a function of two hydro-sedimentary parameters, the Dean number Ω and the Shields number at the breaker point Θ_b. Thus, the bottom typology is represented in the (Ω, Θ_b) diagram for each sand type (Figure 6). We observe the bottom typology strongly depends on Ω and lesser on Θ_b. The dependency on Θ_b decreases with grain size. The three types of sand are similarly organized in terms of Shields number range: $\Theta_b < 0.15$ for the fine-grained sand (Figure 6a), $\Theta_b < 0.22$ for the reference sand (D_{50} = 0.41 mm) (Figure 6b) and $\Theta_b < 0.16$ for the coarser sand (Figure 6c). By cons, an important difference in the range of Ω can be observed (Figure 6). The boundaries are shifted to lower values of Ω for increasing grain diameter. The Ω values range from 1 to 3 for the finest sand (Figure 6a), while they range between 0.5 and 2.5 for the coarse sands (Figures 6b and 6c). Whatever the grain size, we observe that the bottom types and morphologies are similar to those obtained for the reference sand (D_{50} = 0.41 mm). Finally, the classification carried out in this study is robust for a sediment grain size ranging between 0.28 mm and 0.48 mm.

3.2. *Cliff recession rate*

To study the influence of wave forcing on the cliff erosion, we used the reference sand (D_{50} = 0.41 mm) and we analysed the cliff recession as a function of incident wave parameters F and ξ. The spatial and temporal evolution of cliff position is plotted for different values of F (Figure 7a) and ξ (Figure 7b). We can analyse the different phases of the cliff erosion process.

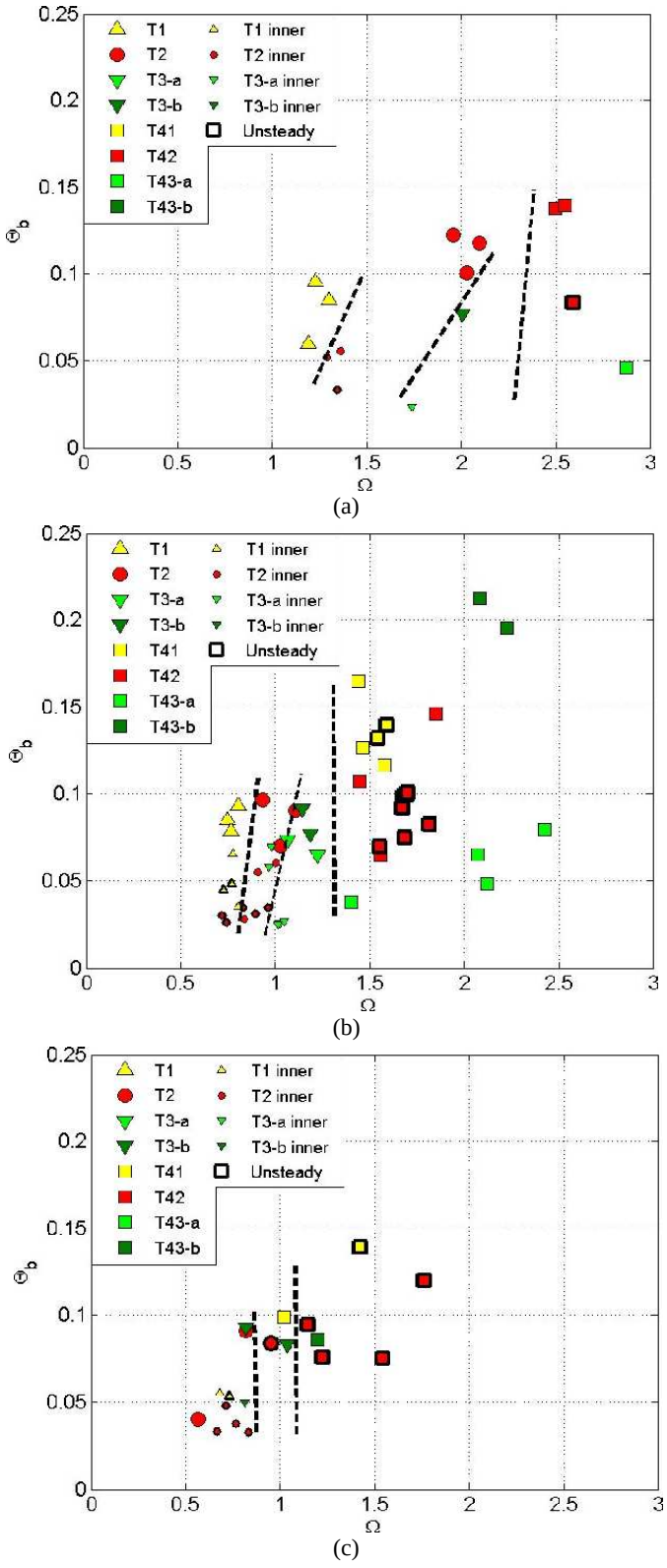

Figure 6. Diagram of bottom typology as a function of (Ω, Θ_b) for different sand types : (a) D_{50} = 0.28 mm, (b) D_{50} = 0.41 mm, (c) D_{50} = 0.48 mm. Representation of symbols are the same as Figure 5.

In Figure 7a, we observe the cliff rapidly stabilizes with increasing F. Indeed, it stabilizes for t ≈ 1-2 h with the stronger values of wave energy flux (F = 2.8-3.2 W/m) and for t ≈ 3-5 h with F < 2 W/m. Moreover, the stabilised cliff position x_C decreases, ie the cliff recession increases, with increasing F. By cons, there is no monotonic tendency as a function of ξ (Figure 7b). For instance, the both cases with the stronger values of ξ (ξ = 0.57-0.67) present at the same time the two extrema of the stabilized cliff position.

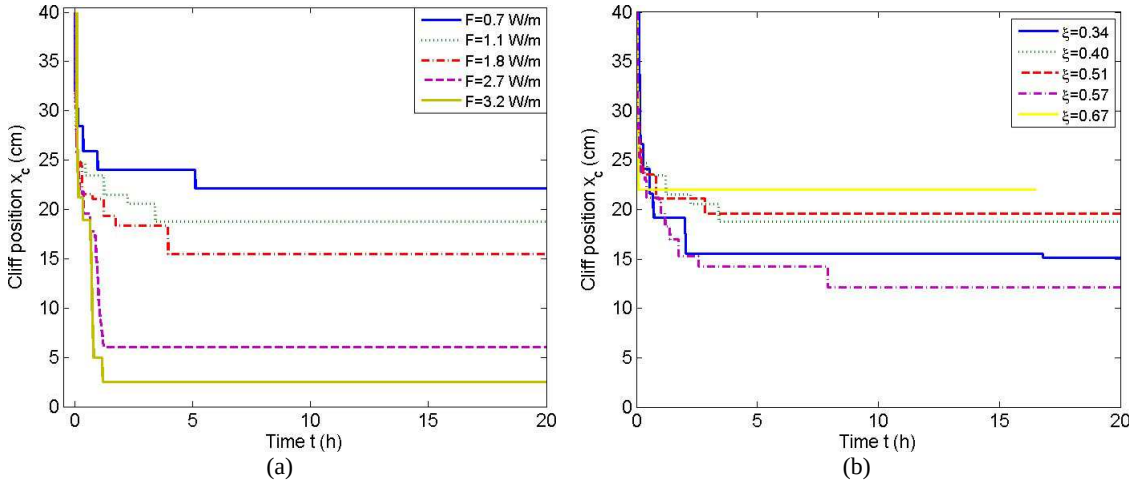

Figure 7. Time evolution of cliff position as a function of: (a) F (for ξ = 0.40) and (b) ξ (for F = 1.1 W/m). The grain diameter of material is D_{50} = 0.41 mm.

For a better analysis of the influence of wave forcing on cliff recession, we chose to define the cliff recession distance D_C and the cliff recession rate R_C when the cliff position is stabilized, they are written:

$$D_C = x_C^S - x_C^i \tag{4}$$

$$R_C = \frac{D_C}{t^S} \tag{5}$$

with x_C^i and x_C^S the initial and stabilized cliff positions and t^S the time when the cliff position is stabilized such as $x_C^S = x_C(t = t^S)$.

These both quantities are represented as a function of the wave energy flux F in Figure 8 and as a function of the surf similarity parameter ξ in Figure 9. We observe the cliff recession distance D_C linearly increases with the wave energy flux F (Figure 8a). Except for the case (ξ, F) = (0.40, 1.8 W/m), the cliff recession rate R_C likewise linearly evolves with F. By cons, there is no monotonic tendency of cliff recession distance (Figure 9a) and rate (Figure 9b) to the surf similarity parameter ξ.

We now analyse the influence of grain diameter of sediment on cliff recession. The grain size change involves a cohesion change of cliff material; indeed a sandy cliff is more cohesive for finer sand. The spatial and temporal evolutions of cliff position with two different grain sizes are represented for two given wave forcing: (ξ, F) = (0.51, 1.1 W/m) (Figure 10a) and (ξ, F) = (0.36, 2.8 W/m) (Figure 10b). Firstly, we can observe in Figure 10 that during the first hours, the cliff position similarly evolves in space and time. Secondly, the stabilized cliff position diminishes for finer sand, thus the cliff recession distance decreases with grain diameter. Indeed, in the first case (Figure 10a), D_C = 22.5 cm for D_{50} = 0.28 mm and D_C = 20.4 cm for D_{50} = 0.41 mm; and in the second case (Figure 10b), D_C = 40 cm for D_{50} = 0.41 mm and D_C = 32.9 cm for D_{50} = 0.48 mm. Finally, contrary to this result, the cliff recession rate increases with the grain diameter of sediment; (i) R_C = 1.4 cm/h for D_{50} = 0.28 mm and R_C = 7.3 cm/h for D_{50} = 0.41 mm in the first case, (ii) R_C = 6.3 cm/h for D_{50} = 0.41 mm and D_C = 10.4 cm for D_{50} = 0.48 mm in the second case. Indeed, the cliff is stabilized faster for coarse sand than for fine sand (Figure 10).

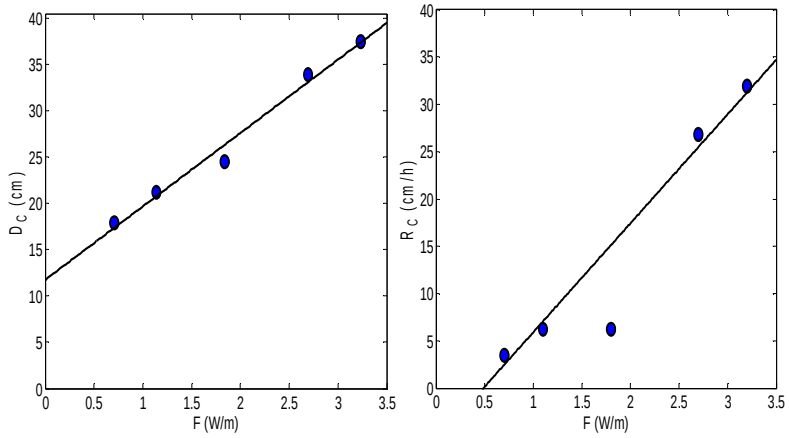

(a) (b)

Figure 8. Cliff recession (a) distance D_C and (b) rate R_C as a function of F (for $\xi = 0.40$).

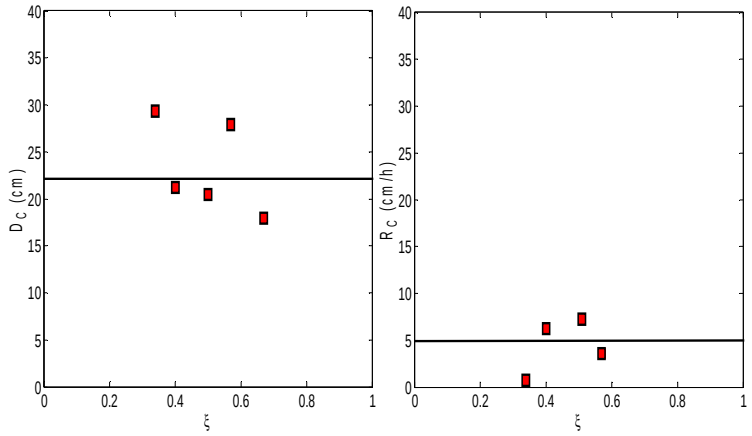

(a) (b)

Figure 9. Cliff recession (a) distance D_C and (b) rate R_C as a function of ξ (for F = 1.1 W/m), the value R_C = 224 cm/h for (ξ, F) = (0.67, 1.1 W/m) is not represented.

4. Discussion

We identified four main bottom morphologies as a function of the shape of the outer platform, (i) steep terrace (type 1), (ii) one-bar profile (type 2), (iii) gentle terrace (type 3) and (iv) double-systems profile with two outer bars (type 4). Breaker type is closely linked to bottom typology (surging, collapsing, spilling and plunging, respectively). Type 4 morphologies present two sub-systems with two distinct breaking waves. The outer system is characterized by a double-bar profile and the inner system corresponds to a type 1, 2 or 3 profile (types 41, 42 and 43). We showed that the bottom typology strongly depends on the surf similarity parameter at the breaker point ξ_b and on the Dean number Ω. This bottom classification is robust for some range of grain sizes (0.28 mm < D_{50} < 0.48 mm). Wright and Short (1984)'s classification shows that the threshold value of Dean number Ω = 1 delimits the bottom profiles of "reflective" (steep beach face) and "intermediate" (bared and terraced) profiles. Our classification matches it: our type 1 profile is "reflective" and types 2-4 are "intermediate". The corresponding threshold value of Dean number is similar to the one obtained by Wright and Short (1984) but slightly changes in function of the sand granulometry ($\Omega \approx$ 0.8-1.3).

We analysed the cliff recession process defining cliff recession distance and rate. We showed the cliff recession distance and rate linearly increase with the wave energy flux and is not monotonic with the surf similarity parameter ξ. However, the bottom morphology changes as a function of ξ, therefore the cliff

recession is directly linked to the type of bottom profile. The influence of grain size of sediment is analysed, even if the cliff is more cohesive for fine sand, the cliff recession distance is lower than for coarse sand. Therefore, the grain size change of the sediment has a more important effect on the wave energy dissipation, through the bottom morphology, than on the cohesion of the cliff material.

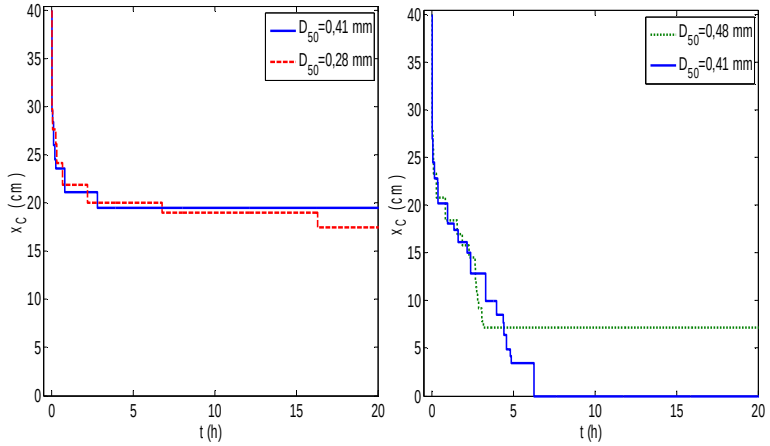

(a) (b)

Figure 10. Time evolution of cliff position as a function of D_{50}: (a) (ξ, F) = (0.51, 1.1 W/m) (b) (ξ, F) = (0.36, 2.8 W/m).

5. Conclusions

An experiment has been conducted to analyze the system behavior and the influence of wave forcing and sediment grain size on bottom morphodynamics and cliff recession. We carried out experiments of sandy cliff erosion by monochromatic wave forcing in a wave flume. We propose a bottom typology based on observed bottom profiles, mostly depending on the surf similarity parameter and the Dean number.
For D_{50} = 0.41 mm, steep terraces with surging breaking waves are observed for $\xi_b > 0.48$ (type 1), one-bared profiles with collapsing breaking waves for $0.42 < \xi_b < 0.48$ (type 2), gentle terraces with spilling breaking waves for $0.38 < \xi_b < 0.43$ (type 3) and two sub-systems profiles for $\xi_b < 0.38$ with two distinct types of breaking waves (type 4). These two sub-systems profiles are composed of a double-bars profile with plunging breaking waves at the outer system and one of the three one-system defined previously as the inner system. The bottom typology is robust for some range of sediment grain size (0.28 mm < D_{50} < 0.48 mm). The bottom type is more dependent on the Dean parameter than the Shields number at the breaker point. Our classification is consistent with the one previously proposed for natural beaches.
We observed the cliff recession linearly increases with the wave energy flux F and is not a monotonic function of the surf similarity parameter ξ, it strongly depends on the bottom type. The grain diameter of sediment plays a role on the bottom morphodynamics and the cohesion of the cliff material. The cliff recession is more important for finer sand even if the cliff is more cohesive, but the cliff recession rate as defined in this work is lower. The cliff recession is directly linked to the bottom dynamics and hydrodynamics associated.

Acknowledgements

We gratefully acknowledge PRES Université de Toulouse for its financial support, as well as Institut National des Sciences de l'Univers (INSU) and SHOM ("Reliefs de la Terre program"), for additional funding of the Rocky cliff erosion project leaded by V.R. We also thank Serge Font, Sébastien Cazin and Hervé Ayrolles for valuable technical assistance.

References

Andrews, C., Williams, R. B. G. 2010. Limpet erosion of chalk shore platforms in southeast England. *Earth Surface Processes and Landforms*, 25, 1371-1381.

Brossard, J., Duperret, A. 2004. Coastal chalk cliff erosion: experimental investigation on the role of marine factors. *Coastal Chalk Cliff Instability, Geological Society, London, Engineering Geology Special Publications*, 20, 109-120.

Caplain, B., Astruc, D., Regard, V., Moulin, F.Y. 2011. Cliff retreat and sea bed morphology under monochromatic wave forcing: Experimental study. *C.R. Geosciences*, 343, 471-477.

Damgaard J.S. and Dong P. 2004. Soft cliff recession under oblique waves: physical model tests. *Journal of waterway, port, coastal and ocean engineering*, ASCE, 234-242.

Emery, K., Kuhn, G. 1980. Sea cliffs: their processes, profiles, and classification. *Geol. Soc. Am. Bull.*, 93, 644-654.

Erikson, L., Larson, M., Hanson, H. 2007. Laboratory investigation of beach scarp and dune recession due to notching and subsequent failure. *Marine Geology*, 245, 1-19.

Grasso, F., Michallet, H., Barthélemy, E., Certain, R. 2009. Physical modeling of intermediate cross-shore beach morphology: Transients and equilibrium states. *Journal of Geophysical Research*, 114.

Kanyaya, J., Trenhaile, A. 2005. Tidal wetting and drying on shore platforms: an experimental assessment. *Geomorphology*, 70, 129-146.

de Lange, W., Moon, V. 2005. Estimating long-term cliff recession rates from shore platform widths. *Engineering Geology*, 80, 292-301.

Pierre, G. 2006. Processes and rate of retreat of the clay and sandstone sea cliffs of the northern Boulonnais (France). *Geomorphology*, 73, 64-77.

Sunamura, T. 1992. Geomorphology of Rocky Coasts. *Wiley, New York.*

Walkden, M., Dickson, M. 2008. Equilibrium erosion of soft rock shores with a shallow or absent beach under increased sea level rise. *Marine Geology*, 251, 75-84.

Wright, L.D., Short, A.D. 1984. Morphodynamic variability of surf zones and beaches: A synthesis. *Marine Geology*, 56, 93-118.

Young, A., Ashford, S. 2008. Instability investigation of cantilevered seacliffs. *Earth Surface Processes and Landforms*, 33, 1661-1677.